Mapping Surface Oil Extent from the Deepwater Horizon Oil Spill Using ASCAT Backscatter

Richard D. Lindsley and David G. Long

Microwave Earth Remote Sensing Laboratory
Brigham Young University
Provo, UT 84602

***Abstract*—The damping effects of oil on capillary ocean waves alter the backscattered power of radar measurements made by remote-sensing instruments such as scatterometers. Numerically computed vector winds are input to a wind geophysical model function (GMF) to determine the predicted backscatter from the ocean surface uncontaminated by surface oil. Large differences between predicted backscatter and measured backscatter indicate areas of the ocean surface potentially affected by oil. The 2010 oil spill from the *Deepwater Horizon* rig in the Gulf of Mexico provides a spatial extent large enough to be mapped by the ASCAT scatterometer. In this paper we use ASCAT data and numerically predicted winds to map the spatial extent of surface oil.**

I. Introduction

The oil spill from the *Deepwater Horizon* oil rig in the Gulf of Mexico is one of the largest environmental disasters in recent history. The consequences from the roughly 4.4 million barrels leaked [1] will continue long after the 15 July 2010 capping of the well. A time-series estimate of the extent and shape of the oil on the ocean surface is beneficial for estimating the amount of oil as a function of time and its effects on ocean life and human industries.

Active microwave sensors are often used for remote detection of oil spills by virtue of their all-weather performance in both day and night conditions. Historically, Synthetic Aperture Radar (SAR) instruments have been used since the spatial resolution—on the order of a hundred meters or less for a spaceborne SAR—is fine enough to resolve many oil spills [2]–[5]. Scatterometers are a related class of active microwave instruments with a resolution that is more coarse—on the order of a few kilometers [6], [7]. The processes that enable oil detection using SAR images are the same for scatterometer data.

The spatial extent of the 2010 Deepwater Horizon oil slick is large enough to be resolvable by the European Space Agency Advanced Scatterometer on MetOp-A (ASCAT), particularly when processed with resolution-enhancement algorithms. By exploiting the effects of surface oil on the radar backscatter from ocean waves, a coarse mapping (resolution $\approx$ 5 km) of oil surface extent is made by examining data processed from ASCAT.

ASCAT is a spaceborne wind scatterometer operating in polar orbit [6]. Like other wind scatterometers, ASCAT indirectly measures near-surface vector ocean winds at a height of 10 meters (U_{10}) by measuring backscattered microwave power over the ocean at various incidence and azimuth angles. An empirically derived geophysical model function (GMF) relates backscatter with U_{10} vector (speed and direction) winds and is used to infer the vector wind from backscatter measurements.

This paper presents a method of mapping surface oil extent by comparing ASCAT-measured backscatter with the predicted backscatter using the GMF and numerical weather predicted (NWP) winds. Background information on ASCAT, the GMF, and the effects of surface oil are presented in Section II. Our methodology for surface oil extent mapping follows in Section III. Results are shown for selected case studies and the performance of the presented method is evaluated in Section IV.

II. Background

Launched in 2006 aboard MetOp-A, ASCAT is in a sun-synchronous polar orbit. It is a real-aperture scatterometer operating in the C-band (5.255 GHz) with three fan beams on either side of the MetOp ground track. This forms approximately a 1820-km-wide ground swath with a 720-km-wide gap at nadir. ASCAT operates in vertical-polarization mode only [6].

The radar backscatter, normalized radar cross-section, or σ°, of the ocean surface is measured by each of the antennas. The CMOD5.n GMF relates σ° as a function of U_{10} and other parameters, including the incidence angle and the azimuth angle relative to wind direction [8].

At the oblique incidence angle range used for scatterometers (30–60° for ASCAT), the scattering mechanism from the ocean surface roughness is due to Bragg scattering. When ocean wave wavelengths of λ_o fulfill the Bragg resonance condition

$$\lambda_o = n\lambda_r/2\sin\theta_i, \quad n = 1, 2, \ldots, \tag{1}$$

where λ_r is the radar wavelength and θ_i is the incidence angle, the electromagnetic waves constructively self-interfere to enhance the surface σ° value [9]. For the radar frequency and range of incidence angles used by ASCAT, ocean waves with a wavelength of 3.5–6.7 cm are primarily responsible for Bragg scattering ($n = 1$).

While modulated by larger gravity waves, Bragg waves are generally in equilibrium with near-surface wind speed [7]. Higher winds generate more Bragg waves, leading to greater σ° values for higher winds. Because oil is more viscous than

sea water, oil on the ocean surface dampens the amplitude of Bragg waves. This modifies the σ° of the affected area because the smoother ocean surface reflects less microwave power back to the scatterometer. The σ° measurement of the oil-contaminated area is thus lower than the oil-free case [2], [4], [10], [11].

The presence of oil in σ° imagery is determined by the contrast difference between oil-affected σ° with non-oil-affected σ°. The value of σ° over the ocean depends on many factors—geophysical, such as near-surface wind speed and direction; instrument-specific, such as the frequency, polarization, and incidence and azimuth angles; and the type and the volume or thickness of surface oil.

While surface oil dominates Bragg wave dampening, other sources can results in patches of dampened backscatter. These include biogenic oil slicks produced by plankton and fish, natural oil seeps from the ocean floor, organic wastes from fish processing ships, and changes in the water-ocean interface, such as that from upwelling [10]. Though covering a much smaller area than the Deepwater Horizon spill, these sources can lead to false positives in oil spill detection, referred to as "look-alikes." Many of these look-alikes are too small to be resolvable by ASCAT. However, low wind speed regions that are large enough to be detected by ASCAT can have very low backscatter and potentially be confused with oil-covered ocean surface.

Another challenge to oil detection is that σ° dampening is wind speed-dependent. If winds are too low ($<$ 3 m/s), the ocean surface is not sufficiently roughened to provide a contrast between the oil-contaminated surface and the oil-free surface. Additionally, if the winds are too high ($>$ 7-10 m/s), the surface oil mixes down into the water and may be less detectable. The wind speed range that is best suited for oil detection is therefore about 3–10 m/s. Previous papers have recognized the importance of factoring wind speed in to surface oil detection [2], [11], and have done so, for example, as part of synergistic data methods [12]. Rather than relying solely upon σ° measurements to detect oil, the method presented in this paper incorporates the effects of wind as part of the detection process. Wind fields from numerical weather prediction (NWP) products are used.

III. Method

Surface oil is detectable given sufficient differences between the observed and predicted backscatter. The predicted backscatter may be determined by computing the GMF based on local wind conditions as approximated by NWP winds.

The backscatter error, or difference between the predicted σ° (from NWP data) and the measured σ° (from ASCAT) is

$$\sigma^\circ_{\mathrm{NWP}} - \sigma^\circ_{\mathrm{ASCAT}} = \epsilon, \tag{2}$$

where ϵ is an error term. While some error is anticipated from noise, the expected value of ϵ is positive in the presence of oil due to the damping effects of the oil on the surface spectrum. Large values of ϵ may be used to detect and map the surface oil extent [13].

A. Predicted backscatter

For comparison wind data, U_{10} from the European Centre for Medium-range Weather Forecasts (ECMWF) are used. ECMWF winds have a temporal resolution of six hours and a spatial resolution of 1°x1°. The two ECMWF wind fields nearest in time to an ASCAT pass over the spill are bilinearly interpolated in space to match the ASCAT measurement locations, and linearly interpolated in time to match the measurement time. The collocated and interpolated NWP wind data is passed through the CMOD5.n GMF to find the σ° value corresponding to the given wind vector, $\sigma^\circ_{\mathrm{NWP}}$.

While this permits a pointwise comparison of $\sigma^\circ_{\mathrm{ASCAT}}$ with $\sigma^\circ_{\mathrm{NWP}}$, linear interpolation low-pass filters the data. The interpolated $\sigma^\circ_{\mathrm{NWP}}$ therefore has limited high-frequency spatial content. With this caveat in mind, a direct comparison of $\sigma^\circ_{\mathrm{ASCAT}}$ with $\sigma^\circ_{\mathrm{NWP}}$ removes the low spatial frequency predicted backscatter from $\sigma^\circ_{\mathrm{ASCAT}}$ but preserves any small-scale structure.

B. Measured backscatter

While a polar-orbiting instrument makes many daily observations of the poles, low-latitude coverage is more sparse. The Deepwater Horizon oil spill is located around 29° latitude, just outside the tropics. A maximum of two passes per day is possible (ascending and descending), but in practice only about eight passes per 10-day period cover the spill region.

For each location in the ASCAT swath, three σ° measurements are collected, one each for the antenna "looks": fore, mid, and aft. The middle look is at a slightly lower range of incidence angles than the fore and aft looks. High resolution σ° imagery is generated for each look using the AVE algorithm. The AVE algorithm is a weighted average of each σ° measurement on a high-resolution grid using estimates of the ground footprint of each measurement [6], [14]–[18]. ASCAT σ° is computed on a 4.45 km by 4.45 km grid using AVE.

C. Backscatter error

Using NWP wind data from ECMWF, the ASCAT measurement geometry (including incidence and azimuth angles), and the GMF, the corresponding $\sigma^\circ_{\mathrm{NWP}}$ is computed for each $\sigma^\circ_{\mathrm{ASCAT}}$ look. Using (2) for each look, the three ϵ errors are represented by the vector $\vec{\epsilon} = [\epsilon_{\mathrm{fore}}\ \epsilon_{\mathrm{mid}}\ \epsilon_{\mathrm{aft}}]^T$. The three looks are combined using the ℓ_2 norm, defined as

$$\|\vec{\epsilon}\|_2 = \sqrt{\epsilon^2_{\mathrm{fore}} + \epsilon^2_{\mathrm{mid}} + \epsilon^2_{\mathrm{aft}}}, \tag{3}$$

which is used as a metric to map the surface oil extent by combining data from all available looks.

D. Oil extent validation

Oil coverage products from the Experimental Marine Pollution Surveillance Report (EMPSR) are used to validate the results. The EMPSR is an experimental product produced by the National Oceanic and Atmospheric Administration (NOAA). Analysts interpret SAR and visible imagery from satellites to estimate the surface oil extent of the spill [19]. EMPSR does not report the oil thickness or volume.

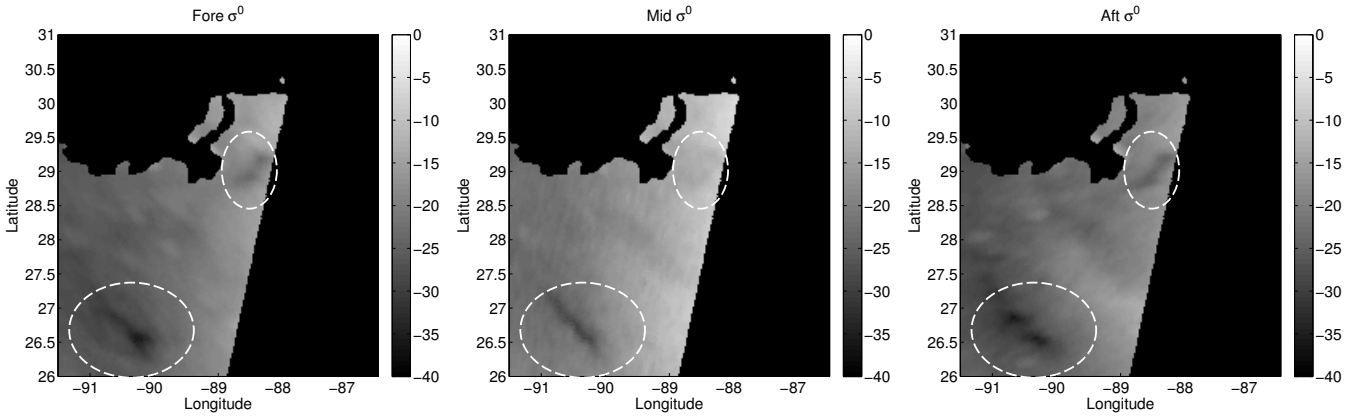

Fig. 1. ASCAT σ° (in dB) fore, middle, and aft looks for rev 19221 (3 July 2010). Fore and aft looks span incidence angles of 36–55° and the middle look spans a range of 27–44°. The fall off of σ° with incidence angle accounts for the brightness variations across the swath. The locations of the two oil spill candidate regions are indicated with dashed ellipses.

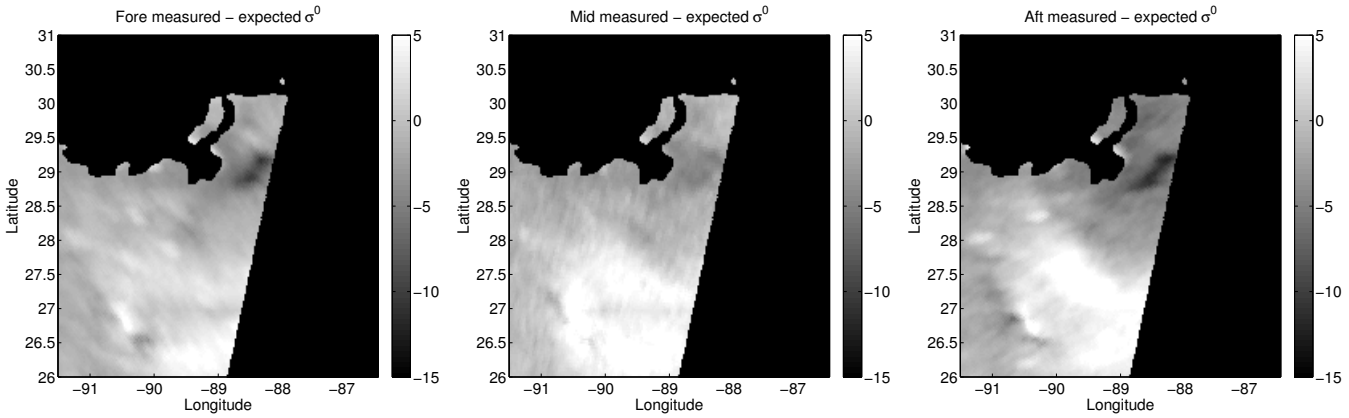

Fig. 2. Difference in dB between measured and predicted σ° for ASCAT rev 19221 (3 July 2010). Compare with Fig. 1. The oil region is not as visible in the mid look due to the different incidence angle between the fore/aft and mid looks.

The EMPSR product used is the daily composite shapefile, a vector-based geospatial representation of surface oil extent based on the available satellite imagery for the day. EMPSR products are not available every day, so only ASCAT passes that coincide with EMPSR data are used.

IV. Results

For the duration of the oil leak (21 April–25 August), 204 ASCAT passes over the spill region are available. Of these, 118 have corresponding EMPSR data, and 11 are selected as case studies. For each ASCAT pass over the oil spill region, the measured σ° for each look is compared with the predicted σ° obtained from interpolated ECMWF winds and the CMOD5.n GMF to obtain the backscatter error. To illustrate the advantage of using NWP winds, we compare the results using both the methodology described above and a method that does not account for winds.

Figure 1 shows the high-resolution σ° field over each of the three looks for an ascending pass of ASCAT. In these images, two potential oil regions can be seen: one east of the Mississippi River Delta and one further south of the delta. The regions are noted with dashed ellipses. Similarly, Fig. 2 shows the difference between the measured and predicted backscatter for each of the three looks. In Fig. 2, the low wind speeds in the region south of the delta are accounted for, leaving only the oil region east of the delta visible.

Without using the predicted backscatter, combining the three looks of Fig. 1 using the ℓ_2 norm results in Fig. 3a. The middle look (center image of Fig. 1) spans a lower incidence angle range than the other two, leading to poor detection of the first oil candidate region. The ℓ_2 norm of the three looks has a greater value for the second candidate region than the first. The second region is a false positive due to low wind speeds in the area.

Incorporating the predicted backscatter and using Eqn. (3) to merge the three looks of Fig. 2 to find the backscatter error results in Fig. 3b. The white outline is the EMPSR product for the day. In this case, the results agree well with the largest EMPSR oil region, while the smaller regions near the coast are not as well detected.

Two other ASCAT passes are shown in Fig. 4a and Fig. 4b. These passes again show a good match with EMPSR results. In general, the EMPSR results corroborate with the method

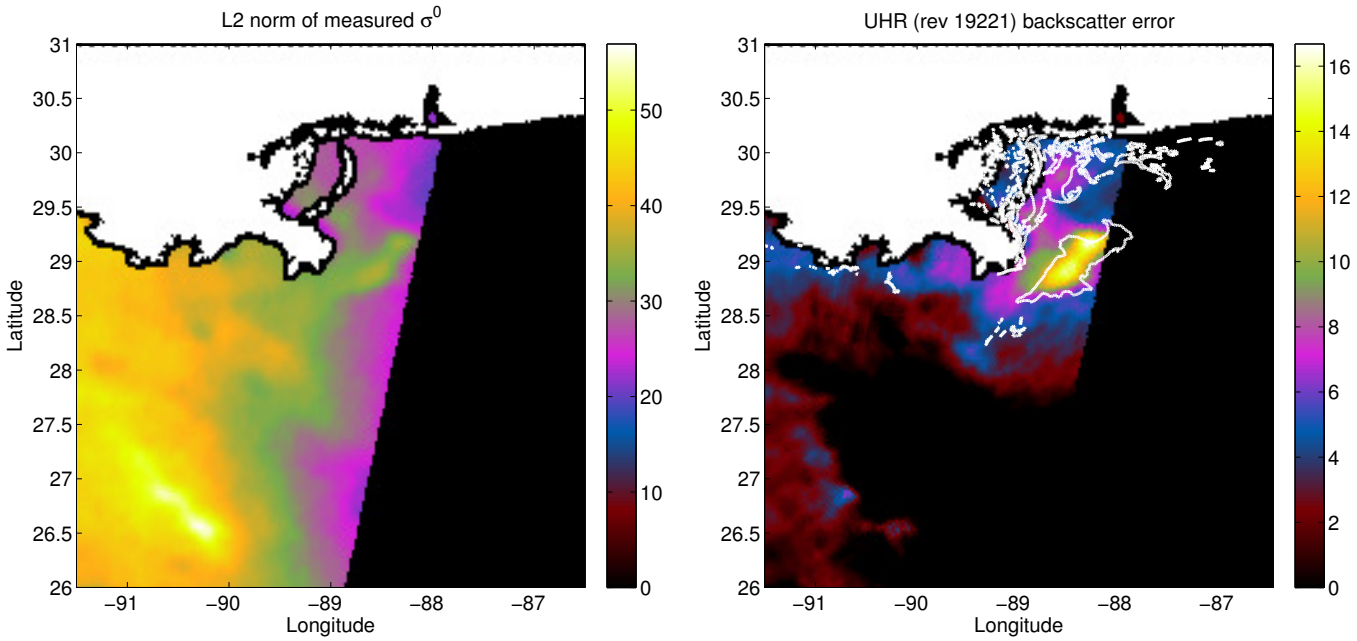

(a) (b)

Fig. 3. The ℓ_2 norm of the measured σ° in (a), and the ℓ_2 norm of the difference between measured and predicted σ° in (b). Data from ASCAT rev 19221 (3 July 2010) is used, along with interpolated ECMWF winds for (b). Land is masked out and near-coastal regions are set to 0 to remove biased wind estimates. The bright area in (b) indicates suppressed σ° measurements due to the presence of surface oil. The white outline is the EMPSR analysis for the surface oil extent.

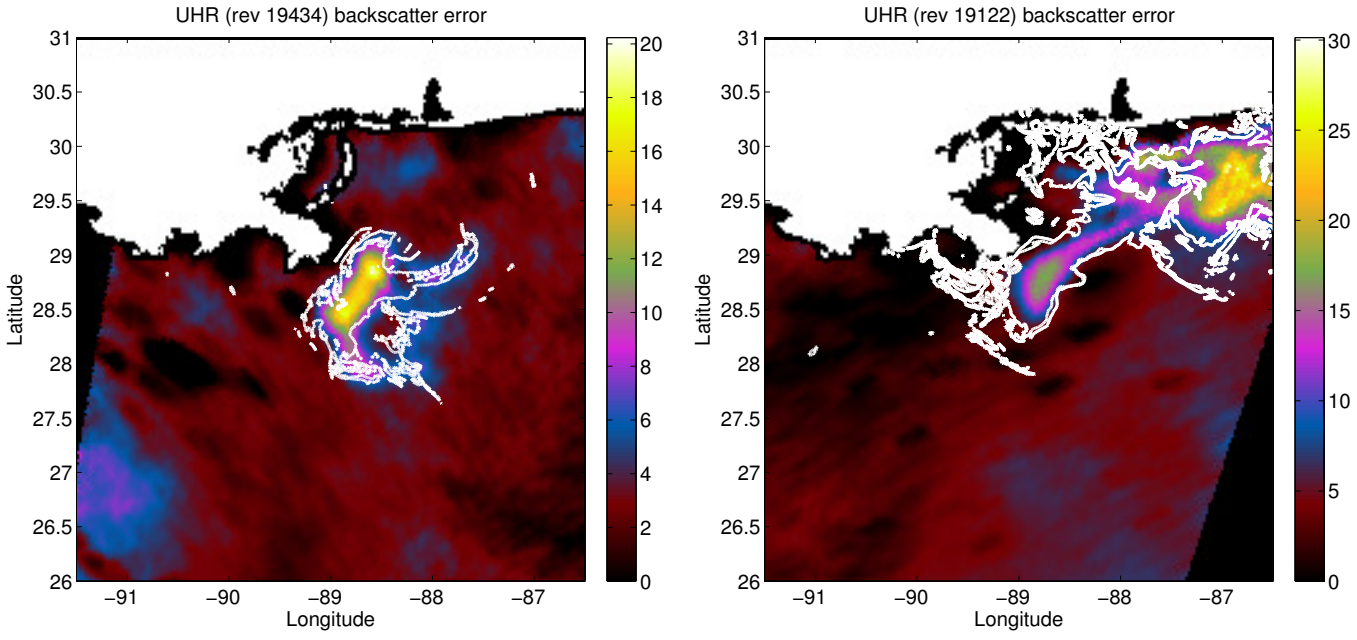

(a) (b)

Fig. 4. Same as Fig. 3b, but (a) is for ASCAT rev 19434 (18 July 2010), and (b) is for ASCAT rev 19122 (26 June 2010).

presented here during the middle of the spill (late April – mid July), but are less effective near the beginning or end of the spill. At these times, the density of surface oil does not appreciably dampen σ°. It appears that at these times, the presence of surface oil does not dampen σ° enough to be detectable by ASCAT. This could be due to the oil collection/burning efforts, weather conditions, or other factors.

V. Conclusion

Though originally designed for only low-resolution global ocean wind measurements, ASCAT can be used to map the surface extent of large bodies of oil on the ocean surface. The detection of ocean surface oil by active microwave instruments is based on a contrast of σ° over oil-affected areas and oil-free areas. Moderate wind speeds sufficiently roughen the ocean surface to provide this contrast. A comparison of σ° values while accounting for the wind over the oil improves the detection.

The method presented in this paper accounts for the near-surface wind by using the ASCAT GMF in conjunction with NWP winds to compute the predicted backscatter, $\sigma^\circ_{\mathrm{NWP}}$. The difference between the predicted backscatter due to the winds and the actual backscatter measured by ASCAT is then evaluated for oil detection, as expressed in Eqn. (2).

The results presented show a good match with conventional oil detection techniques making use of multiple sensors as processed in the EMPSR product. False positives, or oil "look-alikes" still arise owing to the limitations of working with a single instrument, but the occurrence of wind-related false alarms is diminished. Results validate well with EMPSR results except for the very beginning and end of the spill.

References

[1] T. J. Crone and M. Tolstoy, "Magnitude of the 2010 Gulf of Mexico oil leak," *Science*, vol. 330, no. 6004, p. 634, 2010.

[2] C. Brekke and A. Solberg, "Oil spill detection by satellite remote sensing," *Remote Sensing of Environment*, vol. 95, no. 1, pp. 1–13, 2005.

[3] M. Migliaccio, A. Gambardella, and M. Tranfaglia, "SAR polarimetry to observe oil spills," *IEEE Trans. Geosci. Remote Sens.*, vol. 45, no. 2, pp. 506–511, 2007.

[4] M. Migliaccio, F. Nunziata, A. Montuori, X. Li, and W. G. Pichel, "A multifrequency polarimetric SAR processing chain to observe oil fields in the Gulf of Mexico," *IEEE Trans. Geosci. Remote Sens.*, no. 99, pp. 1–9, 2011, Early Access.

[5] A. H. S. Solberg, C. Brekke, and P. O. Husoy, "Oil spill detection in radarsat and envisat SAR images," *IEEE Trans. Geosci. Remote Sens.*, vol. 45, no. 3, pp. 746–755, 2007.

[6] J. Figa-Saldaña, J. J. W. Wilson, E. Attema, R. Gelsthorpe, M. R. Drinkwater, and A. Stoffelen, "The advanced scatterometer (ASCAT) on the meteorological operational (MetOp) platform: A follow on for European wind scatterometers," *Canadian Journal of Remote Sensing*, vol. 28, no. 3, pp. 404–412, 2002.

[7] F. Naderi, M. Freilich, and D. Long, "Spaceborne radar measurement of wind velocity over the ocean-an overview of the NSCAT scatterometer system," *Proceedings of the IEEE*, vol. 79, no. 6, pp. 850–866, 1991.

[8] H. Hersbach, "CMOD5.N: A C-band geophysical model function for equivalent neutral wind," ECMWF, Tech. Rep., 2008. [Online]. Available: http://www.ecmwf.int/publications/library/ecpublications/_pdf/tm/501-600/tm554.pdf

[9] F. Ulaby, R. Moore, and A. Fung, *Microwave Remote Sensing: Active and Passive*, D. Simonett, Ed. Artech House, Inc., 1986, vol. 2.

[10] P. Clemente-Colón and X. Yan, "Low-backscatter ocean features in synthetic aperture radar imagery," *Johns Hopkins APL Technical Digest*, vol. 21, no. 1, pp. 116–121, 2000.

[11] W. Alpers, "Remote Sensing of Oil Spills," in *Maritime Disaster Management Symposium*, 2002, pp. 19–23.

[12] F. Girard-Ardhuin, G. Mercier, F. Collard, and R. Garello, "Operational oil-slick characterization by SAR imagery and synergistic data," *IEEE J. Ocean. Eng.*, vol. 30, no. 3, p. 487, 2005.

[13] R. D. Lindsley and D. G. Long, "Mapping surface oil extent from the Deepwater Horizon oil spill using ASCAT backscatter," *IEEE Trans. Geosci. Remote Sens.*, no. 99, pp. 1–8, 2011, early Access.

[14] ——, "Adapting the SIR algorithm to ASCAT," in *Proc. IEEE Int. Geoscience and Remote Sensing Symp. (IGARSS)*, 2010, pp. 3402–3405.

[15] D. S. Early and D. G. Long, "Image reconstruction and enhanced resolution imaging from irregular samples," *IEEE Trans. Geosci. Remote Sens.*, vol. 39, no. 2, pp. 291–302, 2001.

[16] B. A. Williams and D. G. Long, "Reconstruction from aperture-filtered samples with application to scatterometer image reconstruction," *IEEE Trans. Geosci. Remote Sens.*, vol. 49, no. 5, pp. 1663–1676, May 2011.

[17] M. P. Owen and D. G. Long, "Simultaneous wind and rain estimation for QuikSCAT at ultra-high resolution," *IEEE Trans. Geosci. Remote Sens.*, vol. 49, no. 6, pp. 1865–1878, 2011.

[18] D. G. Long, P. Hardin, and P. Whiting, "Resolution enhancement of spaceborne scatterometer data," *IEEE Trans. Geosci. Remote Sens.*, vol. 31, no. 3, pp. 700–715, 1993.

[19] Satellite Derived Surface Oil Analysis Products - Deepwater Horizon. NOAA/NESDIS. [Online]. Available: http://www.ssd.noaa.gov/PS/MPS/deepwater.html